Ocean Engineering 363 (2026) 126686

Contents lists available at ScienceDirect

Ocean Engineering

journal homepage: www.elsevier.com/locate/oceaneng

Research paper

Experimental and numerical investigation of free-running turning manoeuvres in extreme shallow water

Marcus Döscher [a], *, Carl-Uwe Böttner [a], Moustafa Abdel-Maksoud [b]

[a] Federal Waterways Engineering and Research Institute (BAW), Wedeler Landstr. 157, 22559, Hamburg, Germany
[b] Hamburg University of Technology (TUHH), Am Schwarzenberg-Campus 4, 21073, Hamburg, Germany

ARTICLE INFO

Keywords:
Extreme shallow water
Manoeuvring
DTC
Free-running model tests
Direct manoeuvring simulations
Waterways
Turning circle manoeuvres

ABSTRACT

The precise prediction of ship manoeuvring behaviour in shallow water is essential for safe navigation and waterway design. To examine depth-induced changes in ship dynamics, the turning behaviour of the container ship DTC (Duisburg Test Case) was investigated at model scale (1:60) using combined free-running experiments and CFD simulations, with emphasis on extreme shallow water down to $h/T = 1.10$.

Free-running manoeuvres were conducted, with measurement of propeller thrust and rudder forces. The CFD model was verified by means of a grid convergence study for a complete turning manoeuvre and validated against experimental data, showing mean deviations of approximately 5% for key manoeuvring parameters, confirming its predictive capability.

The results reveal a pronounced deterioration of steady turning performance with decreasing water depth. A reversal in port-starboard asymmetry occurs in shallow water, governed by depth-dependent changes in propeller-rudder interaction and wake distribution. Transient analysis further shows that initial turning ability increases slightly in the transition from $h/T = 1.20$ to 1.15, but deteriorates sharply at $h/T = 1.10$, identifying a critical threshold. These effects are linked to redistributions of hydrodynamic forces along the hull.

The results highlight the coupled influence of water depth and speed, emphasizing the governing role of the depth Froude number on manoeuvring behaviour.

1. Introduction

The continuous growth in the size of seagoing vessels over recent decades has led to increasing operational challenges in port approaches and confined waterways, where water depths and channel dimensions cannot be expanded proportionally. As a result, ships are more frequently required to operate under shallow-water conditions, where manoeuvring performance becomes a critical factor for navigational safety and waterway design. Accident statistics indicate that the majority of maritime incidents occur in coastal and port areas, underlining the importance of understanding ship behaviour in such environments (Li et al., 2006; EMSA, 2022).

It is well established that reduced water depth significantly alters ship manoeuvring characteristics. Numerous experimental investigations have shown that shallow-water conditions generally lead to a deterioration of turning ability, reflected in increased tactical diameters and reduced yaw rates (e.g. Schmidt-Stiebitz, 1958; Lu et al., 1987; Milanov and Chotukova, 2009; Kim et al., 2022). These changes are commonly accompanied by a reduction in drift angle and speed loss during turning manoeuvres (Bogdanov et al., 1987; Lu et al., 1987; Kim et al., 2022). Such effects are typically attributed to increased damping due to enhanced flow confinement in shallow water (Toxopeus, 2013; Lee and Hong, 2017).

While these global trends are well documented, the underlying physical mechanisms governing the change in turning behaviour are still not fully understood. In particular, the redistribution of hydrodynamic forces along the hull with decreasing water depth – and its direct impact on yaw moment development during manoeuvres – has not been systematically analysed.

A wide range of approaches has been applied to investigate shallow-water manoeuvring behaviour, including full-scale trials, model tests, and numerical simulations. Full-scale measurements provide realistic data but are affected by environmental disturbances and high operational costs (Jansch and Böttner, 2019; Jiao et al., 2021). Consequently, free-running model tests are widely regarded as the most reliable experimental method for investigating manoeuvring performance under controlled conditions (ITTC, 2008). These experiments capture

* Corresponding author.
E-mail address: marcus.doescher@baw.de (M. Döscher).

https://doi.org/10.1016/j.oceaneng.2026.126686
Received 27 April 2026; Received in revised form 15 June 2026; Accepted 22 June 2026
Available online 30 June 2026

Nomenclature

β	Drift angle [°]
δ	Rudder angle [°]
Ψ	Heading of the ship [°]
ρ	Water density [kg/m^3]
ϑ	Trimm angle [°]
A_R	Rudder area [m^2]
B_{wl}	Breadth at Waterline [m]
c_B	Block coefficient [–]
C_{X_R}	Longitudinal rudder force coefficient (=$X_R/(0.5U_0^2\rho A_R)$ [–]
C_{Y_R}	Transverse rudder force coefficient (=$Y_R/(0.5U_0^2\rho A_R)$ [–]
D_P	Propeller diameter [m]
GM	Metacentric height [m]
h	Water depth [m]
K_{xx}	Radius of gyration rel. to the x-axis [m]
K_{yy}	Radius of gyration rel. to the y-axis [m]
K_{zz}	Radius of gyration rel. to the z-axis [m]
L_{pp}	Length btw. Perpendicular [m]
N	Hydrodynamic yaw moment [N]
N'	Hydrodynamic yaw moment, non-dimensionalized with $0.5U_0^2\rho L_{PP}^2 T$ [–]
r	Yaw rate [1/s]
r'	Yaw rate, non-dimensionalized (=rL_{PP}/U_0) [–]
S_w	Wetted hull surface [m^2]
T	Mean draught [m]
t	Time [s]
t'	Time, non-dimensionalized (=t U_0/L_{PP}) [–]
T_M	Draught at midship [m]
T_P	Propeller thrust [N]
T_{APP}	Draught at aft perpendicular [m]
T_{FPP}	Draught at forward perpendicular [m]
TC	Turning circle [L_{PP}]
TCR	Turning circle radius [L_{PP}]
TD	Tactical diameter [L_{PP}]
u	Advance speed [m/s]
U_0	Steady straight-ahead advance speed at the start of the manoeuvre [m/s]
UKC	Under keel clearance [–]
V	Displacement Volume [m^3]
v	Sway velocity [m/s]
x_{cg}	Longitudinal centre of Gravity [m]
X_R	Longitudinal rudder force [N]
Y	Hydrodynamic transversal force [N]
Y'	Hydrodynamic transversal force, non-dimensionalized with $0.5U_0^2\rho L_{PP}T$ [–]
Y_R	Transverse rudder force [N]

the ship's dynamic response under free manoeuvring conditions without prescribing a mathematical model and therefore serve as a key reference for both research and engineering applications.

In parallel, Computational Fluid Dynamics (CFD) methods based on Reynolds-Averaged Navier–Stokes (RANS) equations have undergone significant development in the last decade and are increasingly used to analyse manoeuvring flows. Most CFD studies on shallow-water conditions have focused on captive simulations or steady-state manoeuvres, aiming to predict hydrodynamic coefficients or to analyse general flow features (e.g. Toxopeus, 2013; He et al., 2016; Liu et al., 2016; Lee and Hong, 2017; RoyChoudhury et al., 2017; Liu et al., 2019; Wang et al., 2023). Comparisons with experimental data have demonstrated the capability of such approaches to reproduce depth-dependent variations in hydrodynamic forces (Liu et al., 2016, 2019; Ohmori, 2024). However, CFD investigations of self-propelled free-running manoeuvres in shallow water remain limited (Carrica et al., 2016; Kim et al., 2022), primarily due to their high computational cost.

As a result, the link between local flow phenomena and global manoeuvring behaviour is still insufficiently resolved. In particular, a detailed understanding of how shallow-water confinement modifies the spatial distribution of lateral forces along the hull – and how this redistribution governs yaw moment development during turning manoeuvres – is largely missing in the literature.

Furthermore, both experimental and numerical studies have typically been restricted to moderate shallow-water conditions, commonly down to $h/T \approx 1.20$, and often at a single operating speed and draught (Milanov and Chotukova, 2009; Yun et al., 2015; Kim et al., 2022). Consequently, the behaviour of ships in extreme shallow water, as well as the influence of speed-dependent effects, has not been comprehensively investigated. This limitation is particularly relevant since the depth Froude number represents a key governing parameter linking ship speed and water depth, yet its influence on manoeuvring behaviour has rarely been examined systematically.

The present study addresses these gaps by investigating the turning behaviour of a modern container ship under a wide range of shallow-water conditions using a combined experimental and numerical approach. Free-running model tests are conducted at model scale for multiple water depths, extending into the extreme shallow-water regime, and for several operating speeds, draughts, and trim conditions. These experiments provide a comprehensive dataset of global manoeuvring characteristics, including trajectory, yaw rate, and speed evolution.

To complement the experimental analysis, RANS-based CFD simulations of the same manoeuvres are performed to resolve the local flow field and pressure distribution along the hull. This combined approach enables a direct linkage between global manoeuvring performance and the underlying hydrodynamic mechanisms. In particular, the study focuses on identifying how shallow-water effects modify the lateral force distribution and how these changes govern both the initial course-changing behaviour and the steady turning performance.

By integrating detailed experimental data with flow-resolved numerical simulations, the present work provides new insights into the hydrodynamic mechanisms of shallow-water manoeuvring. The results contribute to a more physically grounded understanding of turning behaviour in shallow waters and provide a high-quality reference dataset for the validation of numerical methods and the improvement of manoeuvring prediction models.

2. Experimental investigations

The free-running manoeuvring tests are carried out for the DTC ship model in the test facilities of the BAW in Hamburg. The shallow water tank is 100 m long and 35 m wide. Water levels can be varied up to a maximum level of 0.6 m.

2.1. Model ship

The benchmark ship used in this study is the Duisburg Test Case (DTC), which represents a typical 14,000 TEU post-Panamax container ship (Moctar et al., 2012). The principal particulars of the DTC at both full and model scale (1:60) are given in Table 1. The ship is equipped

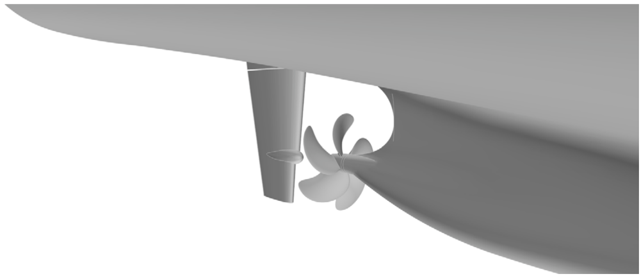

Fig. 1. Perspective view of aft ship with twisted rudder and propeller.

Table 1
Principal particulars of DTC.

Principal particular	Symbols	Full scale	Model scale
Length btw. Perpendicular	L_{pp} [m]	355.00	5.92
Breadth at Waterline	B_{wl} [m]	51.00	0.85
Draught at midship	T_M [m]	14.50	0.242
Displacement Volume	V [m^3]	173 467	0.803
Block coefficient	c_B [–]	0.661	0.661
Wetted hull surface	S_w [m^2]	22 032.00	6.12
Long. centre of Gravity	x_{cg} [m]	174.06	2.90
Metacentric height	GM [m]	3.60	0.06
Moment of Inertia	K_{xx}/B_{wl} [-]	0.41	0.41
Moment of Inertia	K_{yy}, K_{zz}/L_{PP} [-]	0.23	0.23
Propeller (5 bl.) dia.	D_P [m]	8.911	0.149

with a twisted leading edge rudder and a costa bulb, as shown in Fig. 1. The coordinate system of the free running model is illustrated in Fig. 2, where the earth fixed coordinate system x_0, y_0 is aligned with the ship-fixed coordinate system at the beginning of each manoeuvre.

The investigated operating conditions cover model-scale Reynolds numbers based on ship length in the range of approximately 2.6×10^6 to 8.4×10^6. The corresponding full-scale Reynolds numbers range from approximately 1.2×10^9 to 3.9×10^9. For the propeller, the model-scale Reynolds number ranges from approximately 2.4×10^5 to 7.3×10^5, while the corresponding full-scale values range from approximately 8.3×10^8 to 2.5×10^9. The rudder Reynolds number ranges from approximately 6.9×10^4 to 2.2×10^5 at model scale and from approximately 3.2×10^7 to 1.0×10^8 at full scale. These values reflect the typical Reynolds-number discrepancy between model- and full-scale ship manoeuvring investigations. Consequently, model-scale tests exhibit relatively increased viscous effects compared with full-scale conditions. Nevertheless, the Reynolds numbers remain sufficiently high for the investigated operating conditions to be representative of practical ship manoeuvring behaviour, while limiting the overall influence of Reynolds-number scaling effects on the observed manoeuvring characteristics.

2.2. Test conditions

Two draughts were selected for the model tests: the design draught of 14.5 m and a partial draught of 12.5 m. The latter condition was investigated both at even keel and trim by the stern, see Table 2. Experiments were conducted for h/T ratios of 2.00, 1.50, 1.20, 1.15, and 1.10, at test speeds of 6, 9, 12, 15, and 19 knots. The selected speed range reflects realistic operational conditions in the study area. On the River Elbe, vessel speeds are typically restricted to 12 kn over extended navigation reaches, whereas speeds of approximately 6 kn are common during port manoeuvring. Accordingly, 9 kn represents an intermediate regime, whereas 19 kn presents the highest achievable speed for the model without applying skin friction correction force. Fig. 3 shows the DTC during a manoeuvre in the BAW shallow water basin.

Table 2
Main dimensions of investigated floating conditions.

Main particular	Symbol	Design	Partial even	Partial trimmed
Draught at APP	T_{APP} [m]	14.50	12.50	13.50
Draught at midship	T_M [m]	14.50	12.50	12.50
Draught at FPP	T_{FPP} [m]	14.50	12.50	11.50
Trimm angle	ϑ [deg]	0.0	0.0	0.318
Displacement Volume	V [m^3]	173 467	143 640	143 640
Long. centre of Gravity	x_{cg} [m]	174.06	176.10	171.84
Metacentric height	GM [m]	3.60	4.92	4.92

The experimental campaign was conducted using a free-running model ship equipped with a steering gear and an electric motor, operated via remote control. Prior to each test, the model was accelerated to the target speed at the corresponding propeller RPM, after which the RPM was held constant throughout the manoeuvre. At the start of the manoeuvre, the rudder angle was set to the neutral position, and the yaw rate was maintained close to zero to ensure consistent initial conditions. Various manoeuvres were conducted with ranging rudder angles; however, the present paper focuses on the 35° and 45° turning circle manoeuvres. Tests with higher speeds were only feasible under intermediate shallow water condition. For the partial draught, port side manoeuvres were carried out only for 9 kn and for h/T=1.10, the trimmed condition could not be realized.

2.3. Measuring instrumentations

The ship model is equipped with a comprehensive set of onboard measurement systems to capture the relevant manoeuvring parameters, see Fig. 4. Rotational motions of the model, including roll, pitch, and yaw, are measured using a fibre-optic gyro–based motions reference unit (MRU). Hydrodynamic forces and moments acting on the rudder are recorded by a six-degree-of-freedom (6-DoF) load sensor installed in a dedicated sensor box above the rudder blade. Propeller thrust is measured by a three-degree-of-freedom (3-DoF) thrust sensor mounted on the propeller shaft, while the transmitted torque is recorded using an additional rotating torque sensor. The rudder angle is actuated and continuously monitored by an electric steering actuator in combination with a magnetic angle sensor.

Translational motions of the model ship, including surge, sway, and heave, are measured externally via 'total station' positioned next to the shallow water basin. This tachymeter automatically tracks an electronic prism mounted on board the model ship.

An overview of the complete data acquisition system is provided in Fig. 5, which summarizes all measuring instruments employed on the model ship, together with their respective sampling rates and measurement accuracies. Roll motion was monitored throughout all manoeuvres. Maximum transient roll angles remained below approximately 2.7°, while the corresponding steady-state heel angles were generally below 0.5°. The roll response was therefore considered of secondary importance for the present investigation and was not analysed further.

In addition to the sensor accuracies listed in Fig. 5, the overall experimental robustness was assessed through repeated manoeuvres conducted under identical operating conditions. Repeatability was quantified using the coefficient of variation (CV), defined as the ratio of the sample standard deviation to the mean value of the repeated measurements. The CV therefore represents the relative scatter of repeated experiments and provides a measure of experimental repeatability.

The experimental campaign comprised multiple combinations of water depth, velocity, manoeuvre type and turning direction. Reporting repeatability statistics for every individual test condition would result in a substantial increase in the amount of tabulated data while providing limited additional insight into the overall experimental uncertainty. Therefore, Table 3 summarizes the repeatability of the principal manoeuvring parameters by water-depth condition. For each parameter

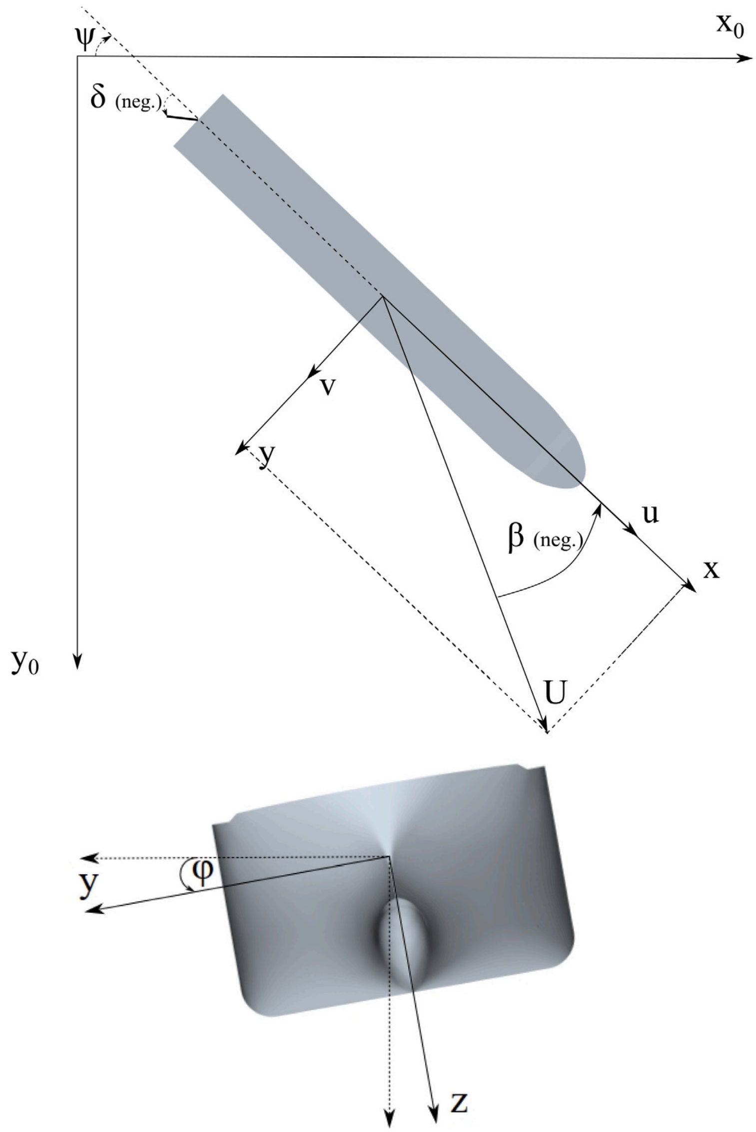

Fig. 2. Coordinate System: top and front view.

Fig. 3. DTC model ship during manoeuvre in the BAW shallow water basin.

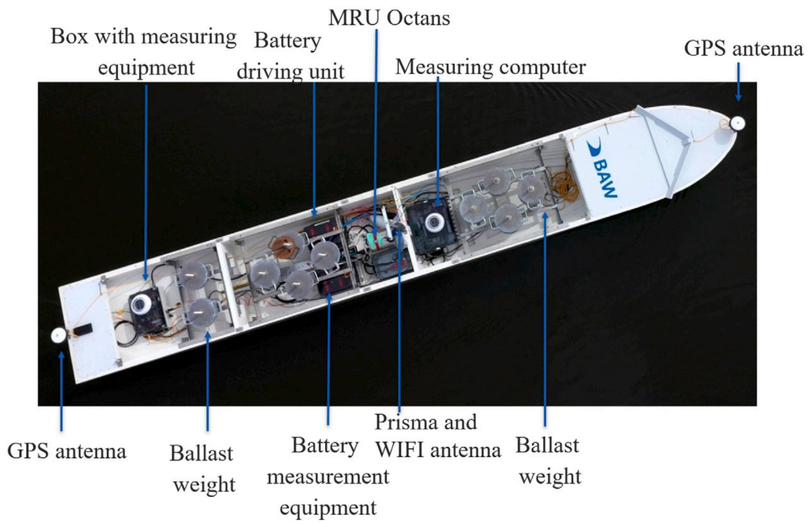

Fig. 4. Fully equipped model ship with measurement applications.

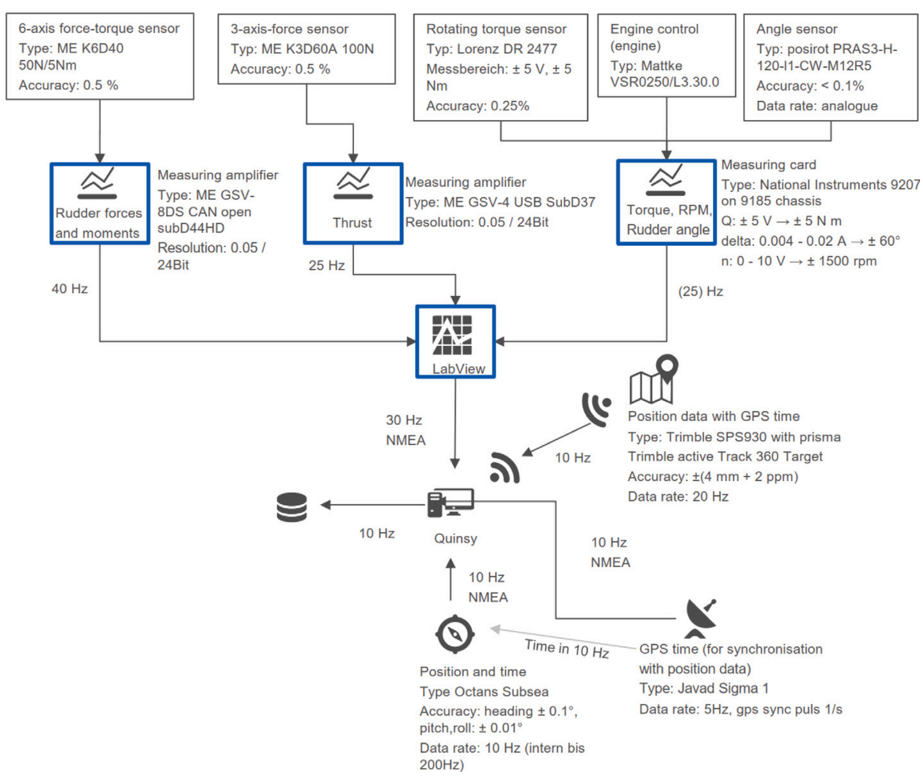

Fig. 5. Central data acquisition diagram.

and h/T ratio, the coefficient CV was first determined from the repeated measurements of the individual test conditions. Subsequently, the resulting CV values from all investigated velocities and both turning directions were combined and characterized by their median and maximum values. The median CV is used as a measure of the characteristic repeatability of the experiments, while the maximum CV represents the largest variability observed within the corresponding water-depth condition. Together, these metrics provide a concise description of both the characteristic and upper-bound repeatability of the experimental database without requiring the presentation of repeatability statistics for every individual test case.

The results indicate a high degree of repeatability of the free-running manoeuvres. As summarized in Table 3, the median coefficient of variation (CV) of the evaluated manoeuvring parameters generally remained below approximately 2.5%, while the maximum observed CV values remained below 4% for all investigated quantities. Similar levels of repeatability were obtained for both trajectory-based and stationary manoeuvring parameters, indicating a high degree of consistency between repeated experiments. Furthermore, no systematic increase in experimental scatter was observed with decreasing water depth. The observed variability is therefore small compared with the hydrodynamic changes induced by the investigated shallow-water conditions, indicating that the reported trends are robust with respect to experimental uncertainty.

Basin-wall effects are assumed to be negligible, as the lateral distance between the ship trajectory and basin boundaries remained at least three times the ship beam. The large dimensions of the manoeuvring basin therefore ensured only minor confinement effects unrelated

Table 3
Repeatability of the model tests for the 35° turning-circle manoeuvre. Repeatability is quantified by the coefficient of variation (CV, %), expressed as the ratio of the sample standard deviation to the mean value of repeated measurements. Median CV values represent the characteristic experimental scatter, whereas maximum CV values indicate the highest variability observed within the experimental database.

Parameter	$h/T = 2.00$		$h/T = 1.50$		$h/T = 1.20$		$h/T = 1.15$		$h/T = 1.10$	
	Median CV	Max CV	Median CV	Max CV	Median CV	Max CV	Median CV	Max CV	Median CV	Max CV
Advance	2.36	2.62	2.00	2.70	1.79	2.78	1.61	3.21	3.18	3.92
Transfer	1.41	3.65	0.97	1.54	0.14	1.84	1.15	2.30	1.97	2.56
t_{90}	1.45	2.76	1.09	2.20	0.82	1.71	0.51	1.01	1.63	2.20
Yaw Rate 90°	1.05	2.11	1.84	2.07	2.14	2.50	1.74	2.41	1.40	1.47
Tactical Diameter	0.87	3.10	0.90	1.66	0.27	0.75	1.16	2.32	–	–
TCR	1.85	3.49	1.12	1.28	0.04	1.36	–	–	–	–
Steady Drift	1.84	2.26	2.08	2.87	1.77	2.66	–	–	–	–
Steady Surge	2.04	2.63	0.69	1.16	1.18	1.78	–	–	–	–
Steady Yaw Rate	0.92	1.85	0.51	1.96	0.28	1.03	–	–	–	–
Steady Rudder Trans. Force	1.20	2.21	1.92	2.12	0.76	2.87	–	–	–	–

to the investigated shallow-water conditions. Remaining uncertainties are mainly associated with the dynamic free-running nature of the experiments and the measurement accuracy of the individual sensors. Nevertheless, the overall consistency of the repeated manoeuvres and the good agreement with CFD results indicate a reliable experimental database for the present investigation.

3. Numerical investigations

In addition to the experimental study, numerical simulations were conducted for conducted manoeuvres of the DTC at model scale, enabling direct comparison with the model tests. The simulations were performed using the RANS solver STAR-CCM+ (version 2302).

3.1. Computational setup

A rectangular computational domain was created based on the CAD geometry of the ship. The domain dimensions were consistent across all setups, except in the vertical direction, which was adjusted to reflect the specific h/T ratios. The domain boundaries included a velocity inlet at the front and side faces, a pressure outlet at the rear, and a symmetry plane at the top, effectively representing a double-body model while neglecting free-surface effects. This simplification considerably reduces computational cost, but neglects free-surface effects such as wave-making and squat. Wave-making effects may become increasingly important at depth Froude numbers approaching critical flow conditions, while squat generally increases with ship speed and decreasing under-keel clearance. In the present study, however, the CFD simulations were limited to comparatively low speeds of 6 and 9 knots full scale, corresponding to Froude numbers of only Fr = 0.052–0.078 and a maximum depth Froude number of Fr_h = 0.37. Consequently, the investigated CFD conditions remain well below the critical shallow-water regime, and free-surface effects are assumed to be of secondary importance for the manoeuvres considered. Preliminary CFD simulations including a free-surface representation did not indicate a significant influence of free-surface effects for the investigated operating conditions. This observation is consistent with the experimental measurements, which showed maximum squat values of approximately 4 mm at 9 kn, corresponding to less than 2% of the model draught.

For deep-water simulations, the bottom was treated as a velocity inlet, whereas for shallow-water conditions, it was treated as a wall to account for seabed confinement (Fig. 6).

Ship motions in surge, sway, and yaw were resolved using the dynamic fluid body interaction (DFBI) model. The background domain moved with the ship to maintain consistent relative motion. The Propeller influence was modelled using a virtual disc with momentum sources applied at the propeller plane, based on open-water k_T–k_Q curves from model tests (Moctar et al., 2012). The local cell velocity was used to compute the advance coefficient J and the corresponding propeller forces, including induced velocity corrections following Neitzel et al. (2015).

The applied actuator-disc approach accounts for both the axial acceleration of the flow and the swirl effect induced by the propeller torque. It therefore provides an efficient representation of the influence of the propulsion system on the flow, as it still accounts for spatially varying inflow conditions at the propeller plane. Since the local cell velocities are used to determine the advance coefficient, asymmetric wake distributions and depth-dependent inflow variations caused by manoeuvring motion and shallow-water effects are inherently included in the propeller loading. Consequently, the simulations are able to capture the dominant changes in propeller–rudder interaction associated with altered wake fields in shallow water.

Nevertheless, the simplified propulsion model does not resolve detailed blade-scale flow phenomena such as tip and hub vortices. Therefore, local interaction effects between propeller and rudder may not be represented with the same fidelity as in fully resolved propeller simulations. A fully resolved rotating propeller would furthermore require substantially smaller time steps and significantly higher computational effort, particularly for the long-duration free-running manoeuvring simulations performed in the present study.

In addition, the employed open-water k_T and k_Q characteristics correspond to deep-water conditions. While shallow water may slightly influence the open-water propeller characteristics themselves, these effects are assumed to be secondary compared to the substantially larger changes in hull wake and inflow distribution caused by shallow-water confinement, which are directly resolved by the CFD simulations.

The rudder was independently controlled using an overset grid region. While the remainder of the domain employed a trimmed-cell mesh, the rudder geometry was discretized with a polyhedral mesh for accurate resolution. The total cell count for the DTC simulations was 11.9 million, with 36 prism layers along the hull to properly capture the boundary layer ($y^+ < 1$). Fig. 7 shows some different perspectives of the used mesh.

Turbulence was modelled using the low-Re Standard k–ϵ formulation, which was found to best reproduce the validation data for the DTC. Convective terms were discretized using a second-order upwind scheme, and transient terms were solved implicitly using a first-order backward Euler method. The time step was chosen to maintain a Courant number below one in most of the domain, allowing slightly higher values near the propeller and rudder where local mesh refinement would otherwise impose prohibitively small steps.

3.2. Verification

The numerical results were verified through a systematic grid convergence and uncertainty analysis following the methodology of Xing and Stern (2010), ITTC (2024). Three mesh resolutions were considered: coarse, medium, and fine, with a refinement ratio of $r = \sqrt{2}$.

For steady conditions, verification was performed using shallow-water resistance data at 6 kn for three representative water depths:

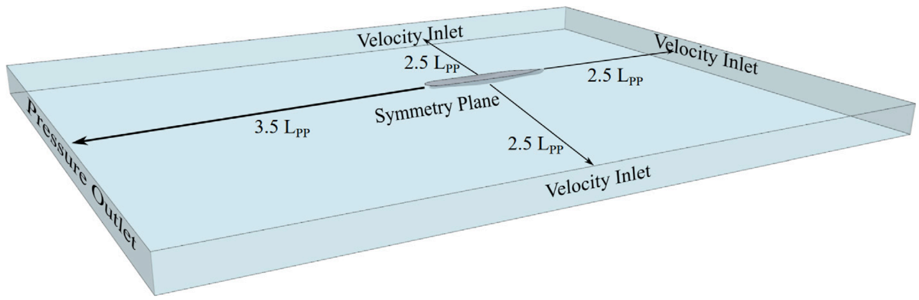

Fig. 6. Principle boundary conditions used for the numerical simulations.

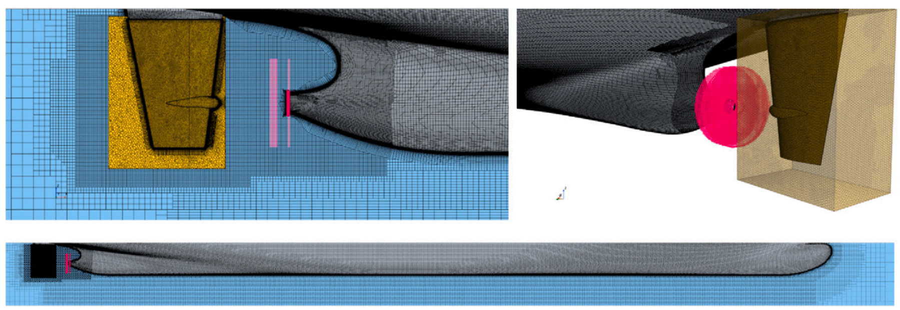

Fig. 7. Different perspectives of the computational mesh for the DTC.

Table 4
Grid convergence study based on resistance tests.

Total cells Water depth	Coarse 5.5×10^6	Medium 11.9×10^6	Fine 20.8×10^6	ε_{21}	ε_{32}	R	δ_{RE}	U_{FS}
Deep water	$C_{TM}(10^{-3})$ [–]							
	4.5682	4.5555	4.5547	0.0009	0.0126	0.0689	0.0001	0.0031
$h/T = 2.00$	4.8829	4.8617	4.8617	0.0001	0.0211	0.0039	3.1867E−07	0.00004
$h/T = 1.20$	5.8492	5.8156	5.7991	0.0165	0.0336	0.4915	0.0159	0.032

Table 5
Grid convergence study based on a 35° turning circle manoeuvre at $h/T = 1.50$.

Parameter	Coarse	Medium	Fine	ε_{21}	ε_{32}	R	δ_{RE}	U_{FS}	Convergence type
Advance [L_{PP}]	2.5410	2.5098	2.5450	−0.0352	0.0312	−1.1277	0.3107	0.8070	Oscillatory Diverging
Transfer [L_{PP}]	1.5663	1.5743	1.5726	0.0017	−0.0080	−0.2145	0.0005	0.0101	Oscillatory Converging
t_{90} [–]	4.0241	4.0283	4.0287	−0.0004	−0.0042	0.0970	0.0000	−0.0018	Monotonically Converging
Tactical Diameter [L_{PP}]	3.5466	3.5604	3.5549	0.0056	−0.0138	−0.4024	0.0038	0.0253	Oscillatory Converging
TCR [L_{PP}]	1.7115	1.6817	1.7010	−0.0193	0.0298	−0.6454	−0.0351	−0.0671	Oscillatory Converging
Steady Surge [–]	0.5879	0.5599	0.5769	−0.0170	0.0280	−0.6075	−0.0263	−0.0484	Oscillatory Converging
Steady Thrust [–]	0.0292	0.0295	0.0294	0.0002	−0.0003	−0.5516	0.0002	0.0004	Oscillatory Converging
Steady Drift [°]	8.2505	8.1641	8.1307	0.0334	0.0865	0.3857	0.0209	0.1621	Monotonically Converging
Steady Drift 90° [°]	8.3733	7.8150	8.3466	−0.5316	0.5584	−0.9521	−10.5600	−25.2360	Oscillatory Converging
Steady Sway [–]	−0.0852	−0.0803	−0.0824	0.0021	−0.0049	−0.4262	0.0016	0.0084	Oscillatory Converging
Steady Yaw Rate [–]	0.3471	0.3374	0.3427	−0.0052	0.0096	−0.5422	−0.0062	−0.0105	Oscillatory Converging
Yaw Rate 90°	0.3713	0.3676	0.3726	−0.0049	0.0037	−1.3450	0.0192	0.0539	Oscillatory Diverging
Steady Rudder Trans. Force [–]	−0.0084	−0.0085	−0.0085	0.0000	0.0001	−0.0959	0.0000	0.0000	Oscillatory Converging
Rudder Trans. Force 90° [–]	−0.0080	−0.0082	−0.0082	−0.0001	0.0002	−0.4110	−0.0001	−0.0003	Oscillatory Converging

deep water, moderate shallow water ($h/T = 2.00$), and shallow water ($h/T = 1.20$). In addition, a 35° turning circle manoeuvre at 9 kn and $h/T = 1.50$ was simulated to assess the convergence of transient manoeuvring results.

Grid convergence was evaluated using the relative differences between meshes, $\varepsilon_{21} = S_2 - S_1$ and $\varepsilon_{32} = S_3 - S_2$, following Xing and Stern (2010). The convergence ratio $R = \varepsilon_{21}/\varepsilon_{32}$ was used to classify the convergence behaviour. δ_{RE} denotes the estimated discretization error based on Richardson extrapolation, while U_{FS} represents the numerical uncertainty obtained using a safety-factor approach. The results indicate monotonic convergence for steady resistance coefficients, with estimated uncertainties of approximately 0.07,%, 0.0008,%, and 0.55,% of C_{TM} for deep water, $h/T = 2.00$, and $h/T = 1.20$, respectively (see Table 4).

For the turning circle manoeuvre, verification parameters included standard manoeuvring metrics (e.g., tactical diameter, advance, and drift angle), as well as rudder and propeller forces and velocities, see Table 5. Most parameters exhibited oscillatory convergence, with the exceptions of the time to 90° heading change (t_{90}) and steady-state drift angle, which demonstrated monotonic convergence. The advance and yaw rate at 90° heading change showed minor oscillatory divergence, with R values remaining within 12–35,% of the limit of −1. These results highlight the inherent challenges of applying classical grid convergence approaches to unsteady manoeuvring simulations (Carrica et al., 2016).

Table 6
Results of the resistance and propulsion tests for EFD and CFD.

h/T	Resistance			Propulsion		
	EFD $c_T(10^{-3})$	CFD $c_T(10^{-3})$	Deviation c_T [%]	EFD k_T	CFD k_T	Deviation k_T [%]
4.00	4.6181	4.5556	−1.35	0.2727	0.2624	−3.77
2.00	5.1620	4.9109	−4.86	0.3010	0.2810	−6.64
1.20	6.4608	5.8742	−9.08	0.3407	0.3232	−5.13

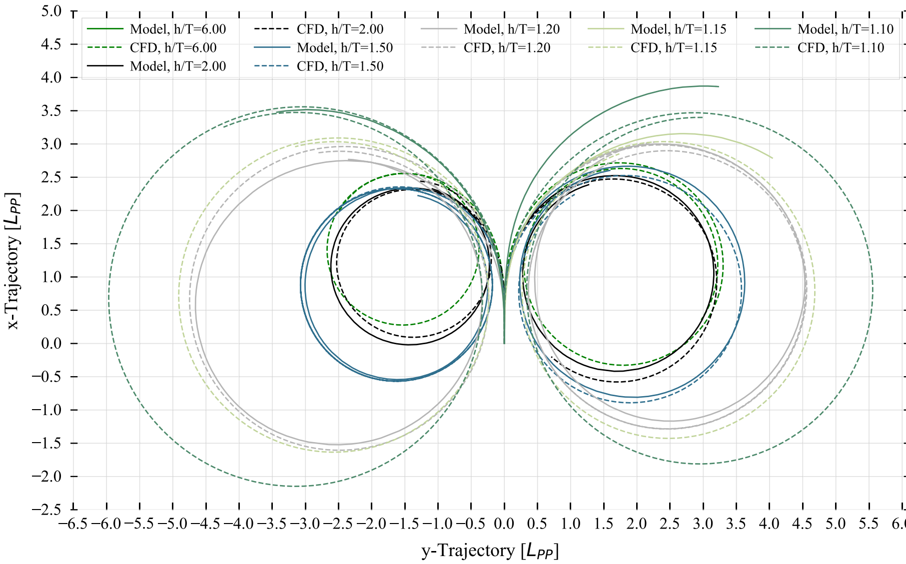

Fig. 8. Comparison of EFD and CFD trajectories for the 35° turning circle manoeuvre with an initial speed of 9 kn.

Overall, the uncertainty analysis confirms that the chosen medium-resolution mesh provides a reliable balance between accuracy and computational cost for the DTC manoeuvres investigated.

3.3. Validation

The numerical results for the DTC were validated against the corresponding free-running model tests conducted in the BAW shallow-water basin. Steady resistance and propulsion tests at 6 kn were used to benchmark CFD predictions in deep water, moderate shallow water ($h/T = 2.00$), and shallow water ($h/T = 1.20$). The comparison, summarized in Table 6, shows that CFD slightly underestimates both resistance and propeller thrust, with deviations below 10%. The largest discrepancy occurs for shallow-water resistance (≈9%), corresponding to an absolute difference of only 0.27 N due to the low total resistance at this speed.

Direct manoeuvring simulations were validated using 35° turning circle manoeuvres at 9 kn. Main manoeuvring metrics (e.g. advance, tactical diameter, transfer) and dynamic parameters (e.g. yaw rate, rudder force) were compared with model test data. These quantities were selected to represent both the transient and steady-state phases of the manoeuvre and to provide a compact validation of the predicted ship-motion response. CFD trajectories generally reproduce the experimental paths accurately, including in extreme shallow-water conditions, where the model experiments were limited (Fig. 8).

Parameters corresponding to 90° heading change also show good agreement (Fig. 9). Transfer, yaw rate, and time to 90° heading change closely match the experimental data for all water depths, with the largest deviation observed for the starboard manoeuvre at $h/T = 1.15$ (≈ 14% in transfer). Advance is slightly overestimated for port-side turning at $h/T = 1.20$, and slightly underestimated for starboard turning, particularly under extreme shallow-water conditions ((≈11.6%). Overall, the trends with decreasing water depth are well captured.

Steady-state parameters, including tactical diameter, steady yaw rate, rudder transverse force, surge velocity, and drift angle, were also compared (Fig. 10). Tactical diameter and steady yaw rate agree within 5% and 10% respectively, for all comparable conditions. Slightly higher deviations are observable for rudder transverse force (up to (≈20%) under moderate shallow-water conditions. Steady drift angles are well represented for starboard turns, while deviations for port-side turns reach over 20% at $h/T = 1.20$, though absolute differences remain below 1° in shallow water. For surge velocity, good overall agreement is obtained, with deviations around 2% for starboard turning and up to 5% for port turning at $h/T = 1.50$ and 1.20. A somewhat larger deviation of about 11% is observed for the port turning case at $h/T = 2.00$. The CFD simulations correctly capture the characteristic trend reversal in turning circle radius and tactical diameter when transitioning from moderate to shallow water.

A comprehensive comparison of all manoeuvring parameters is summarized in Table 7. The mean absolute error across all parameters remains close to 5%, indicating that the CFD setup provides a reliable representation of the DTC turning circle behaviour across the investigated shallow-water conditions.

4. Results and discussion

The experimental and numerical results of the shallow-water manoeuvres are presented and analysed in the following. In addition to trajectories, motions, and measured forces, the standard parameters of turning circle manoeuvres are evaluated.

The analysis is structured to first examine the influence of water depth and depth Froude number at design draught conditions, followed by the effect of modified loading conditions.

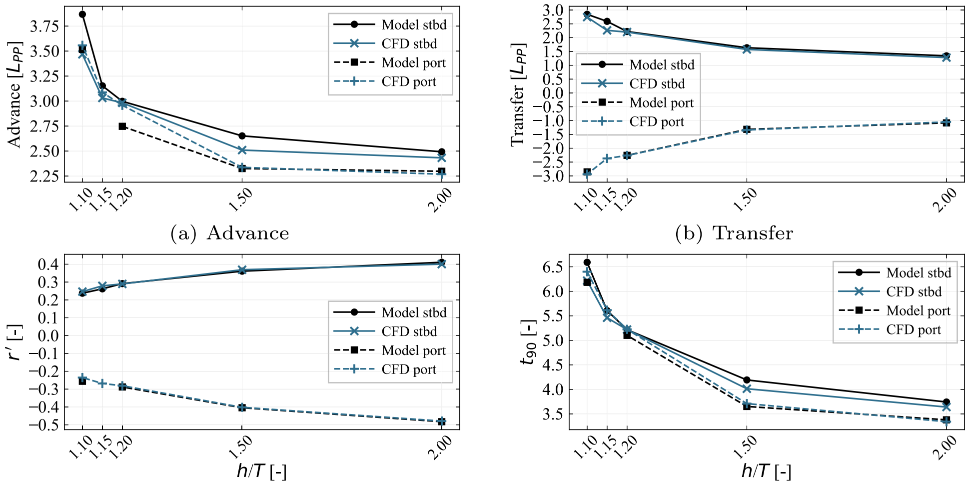

(a) Advance (b) Transfer

(c) Yaw Rate at 90° Heading (d) Turning Time at 90° Heading

Fig. 9. Validation plots for turning parameters related to 90° heading change with an initial speed of 9 kn.

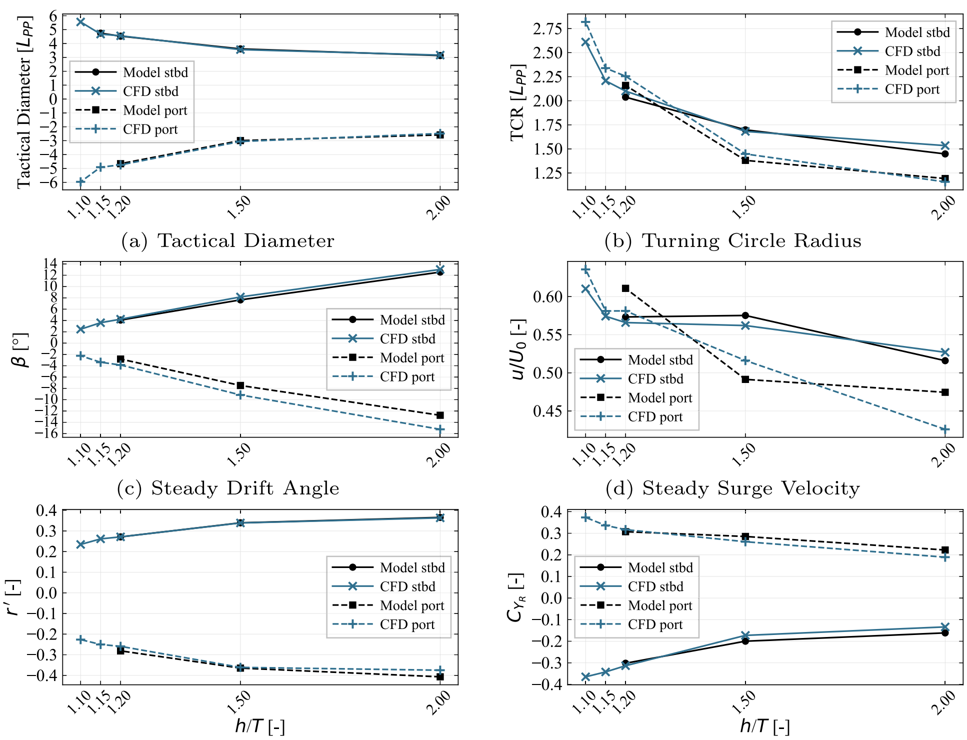

(a) Tactical Diameter (b) Turning Circle Radius

(c) Steady Drift Angle (d) Steady Surge Velocity

(e) Steady Yaw Rate (f) Steady Transverse Rudder Force

Fig. 10. Validation plots for steady-state turning parameters with an initial speed of 9 kn.

4.1. Influence of depth froude number on manoeuvring behaviour at design condition

Given the wide range of investigated water depths and speeds, the results are primarily presented as a function of the depth Froude number to capture the combined influence of velocity and water depth. For each h/T ratio, second-order polynomial regression curves are included to indicate overall trends.

Shallow-water conditions are classified according to ITTC (2014, 2021) and PIANC (1992), with $h/T > 4.00$ representing deep water, $h/T = 2.00$ and 1.50 moderate shallow water, $h/T = 1.20$ shallow water, and $h/T = 1.15$ and 1.10 extreme shallow water.

Turning circle manoeuvres were performed at rudder angles of 35° and 45°. The 35° manoeuvres cover speeds from 6 to 19 kn, depending on the available under-keel clearance, while the 45° cases were conducted at 6 and 9 kn. At very low h/T ratios, limitations in basin dimensions prevented the completion of full turning circles; see Fig. 11. Since most standard manoeuvring parameters are defined in the steady phase, the analysis focuses first on steady-state behaviour.

The trajectories of the 35° turning circle manoeuvres (Fig. 11) clearly show a significant increase in the measured tactical diameter and turning radius with decreasing h/T. This trend is quantified in Fig. 12, where both parameters increase monotonically as under-keel

Table 7
Differences between CFD and EFD results of the 35° turning circle manoeuvre in %.

Parameter	h/T = 2.00	h/T = 1.50	h/T = 1.20	h/T = 1.15	h/T = 1.10
Advance stbd	−2.48	−5.66	−0.53	−4.01	−11.55
Advance port	−1.30	0.50	7.11	–	1.14
Transfer stbd	−4.90	−3.87	−0.90	−14.38	−3.76
Transfer port	−3.13	1.58	0.18	–	2.85
t_{90} stbd	−2.82	−4.47	0.04	−2.67	−6.01
t_{90} port	−1.13	1.57	2.36	–	3.39
Yaw Rate 90° stbd	−2.55	2.20	−0.58	5.99	3.68
Yaw Rate 90° port	−0.75	−0.55	−2.41	–	−8.84
Tactical Diameter stbd	1.03	−1.46	0.56	−1.46	–
Tactical Diameter port	−4.03	2.10	1.81	–	–
TCR stbd	5.64	−0.99	2.99	–	–
TCR port	−2.96	4.60	4.24	–	–
Steady Drift stbd	3.64	6.37	3.75	–	–
Steady Drift port	16.28	18.26	27.12	–	–
Steady Surge stbd	2.09	−2.35	−1.31	–	–
Steady Surge port	−11.40	4.79	−5.08	–	–
Steady Yaw Rate stbd	−0.60	−0.21	0.05	–	–
Steady Yaw Rate port	−8.54	−0.94	−8.43	–	–
Steady Rudder Trans. Force stbd	−20.76	−15.58	3.66	–	–
Steady Rudder Trans. Force port	−17.59	−9.32	3.01	–	–
Mean Error	5.68	4.37	3.81	5.70	5.15

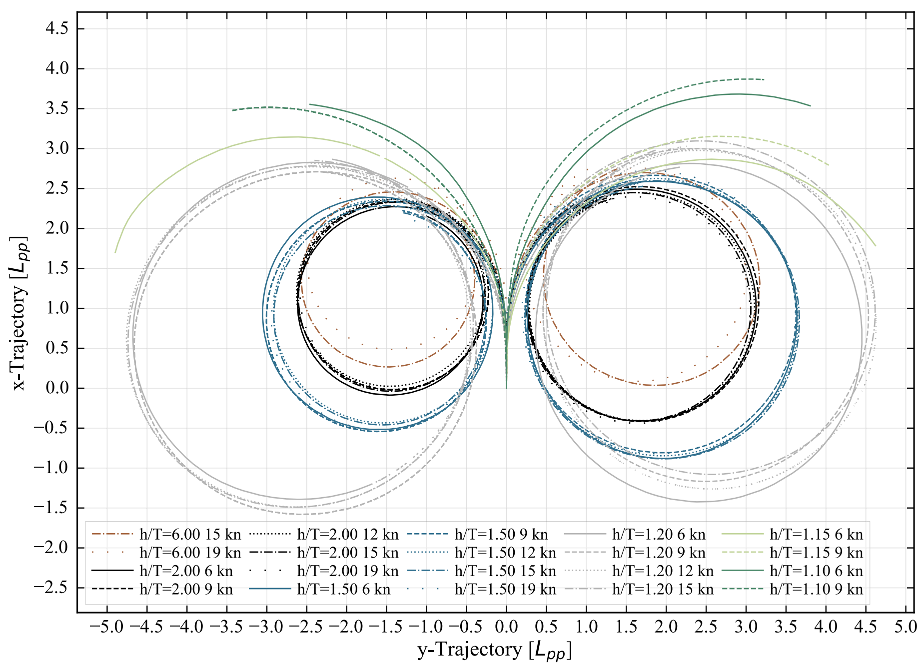

Fig. 11. Trajectories of the 35° turning circle manoeuvre.

clearance decreases. The gradient of this increase becomes more pronounced towards extreme shallow-water conditions, indicating a strong deterioration of turning ability.

The dependence on speed remains relatively weak, as indicated by the nearly horizontal regression curves over the depth Froude number. Only in shallow and extreme shallow water a more pronounced speed influence emerges. In particular, the advance increases noticeably with increasing depth Froude number for starboard turning in the range $Fr_h \approx 0.25$–0.38, while remaining nearly constant for port turning. Along constant-speed curves, the increase in advance becomes especially significant under shallow and extreme shallow-water conditions (Fig. 12).

A distinct increase in advance is observed in the transition from $h/T = 1.15$ to 1.10, representing the strongest change across all investigated depths. This highlights the sensitivity of the initial turning behaviour to extreme shallow-water conditions.

To better distinguish the observed manoeuvring trends from their physical interpretation, the underlying hydrodynamic mechanisms are discussed separately in the following. The increase in turning-circle parameters is primarily attributed to enhanced hydrodynamic damping with decreasing under-keel clearance. This increased damping reduces the drift angle, which in turn affects both resistance and speed during the manoeuvre. The steady drift angle and surge velocity show consistent trends across all speeds. While the drift angle varies only weakly with depth Froude number, the surge velocity exhibits a non-linear behaviour: it decreases initially and increases again at higher depth Froude numbers. The onset and magnitude of this increase depend strongly on h/T, shifting to lower depth Froude numbers and becoming more pronounced as water depth decreases.

Since the drift angle does not capture this non-linearity, the observed behaviour is instead attributed to the interaction between the propeller and the rudder. The rudder forces shown in (Fig. 12) exhibit a similar dependence on depth Froude number as the model speed. As

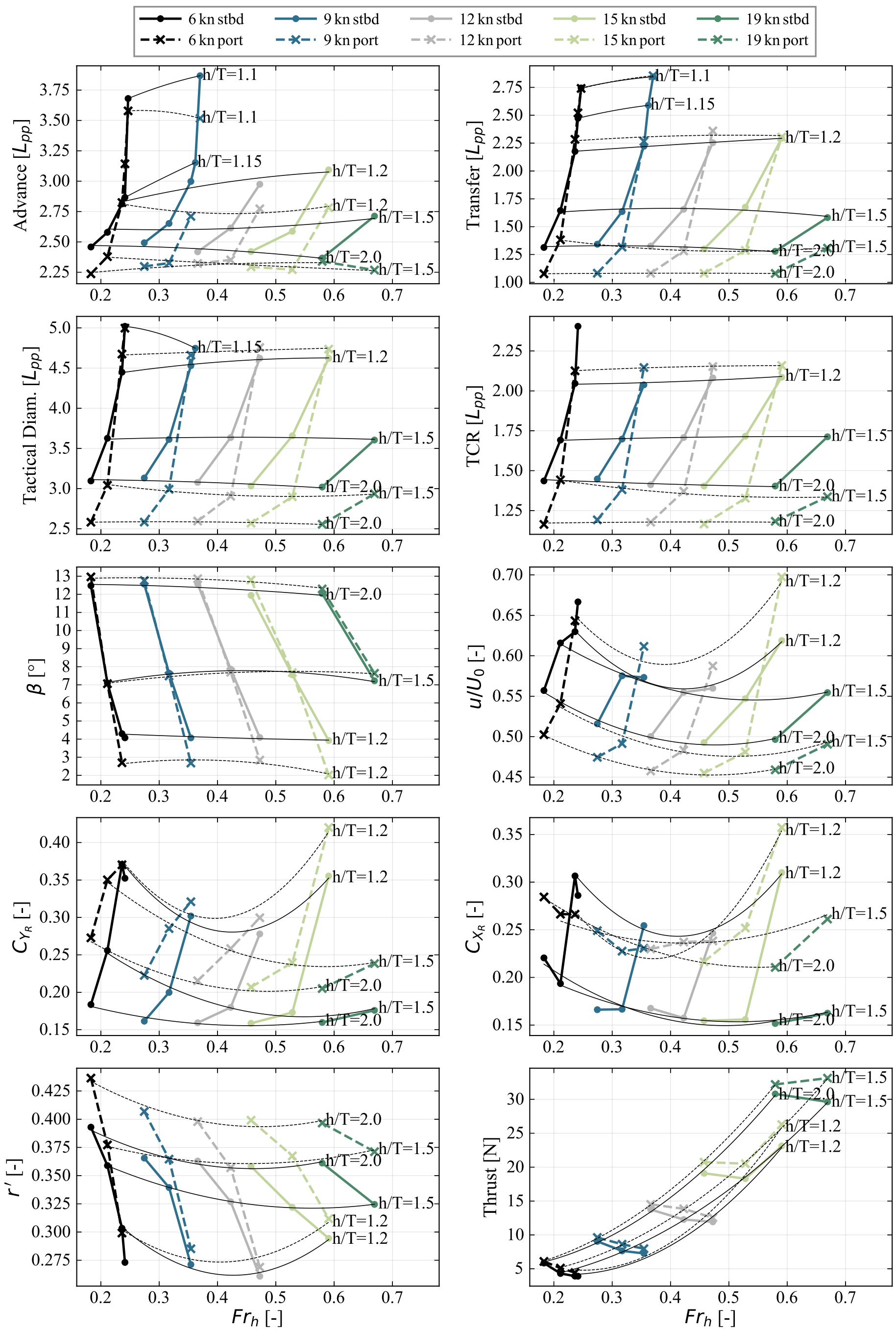

Fig. 12. Turning circle parameters.

the under-keel clearance decreases, a larger portion of the rudder area is exposed to the propeller slipstream velocity, leading to an increase in rudder force. This modified rudder inflow results in a strong coupling between rudder–propeller interaction and velocity development during the manoeuvre. The resulting non-linear rudder force response directly governs the velocity loss during the manoeuvre.

This is further supported by the magnitude of the rudder forces: at 15 kn, both longitudinal and transverse components increase significantly between h/T = 1.50 and 1.20, exceeding 100% for starboard turning and reaching approximately 40–70% for port turning. At lower speeds, the increase is less pronounced, highlighting the combined influence of speed and water depth.

The propeller thrust during steady turning (Fig. 12) reflects the same non-linear behaviour. In moderate shallow water, thrust decreases initially, while at higher speeds a marked increase occurs when transitioning to shallow water. This behaviour results from competing effects: increasing wake fraction enhances propeller loading, while higher effective advance speed reduces it. Additionally, reduced oblique inflow in shallow water modifies the propeller inflow conditions. The balance of these effects leads to a strongly non-linear thrust response, particularly at higher speeds.

The steady yaw rate decreases with decreasing h/T, consistent with the overall increase in hydrodynamic damping. Its dependence on depth Froude number follows a similar pattern to the surge velocity, with a non-linear variation that correlates closely with the transverse rudder force. This again underlines the dominant role of stern flow interaction in governing manoeuvring behaviour.

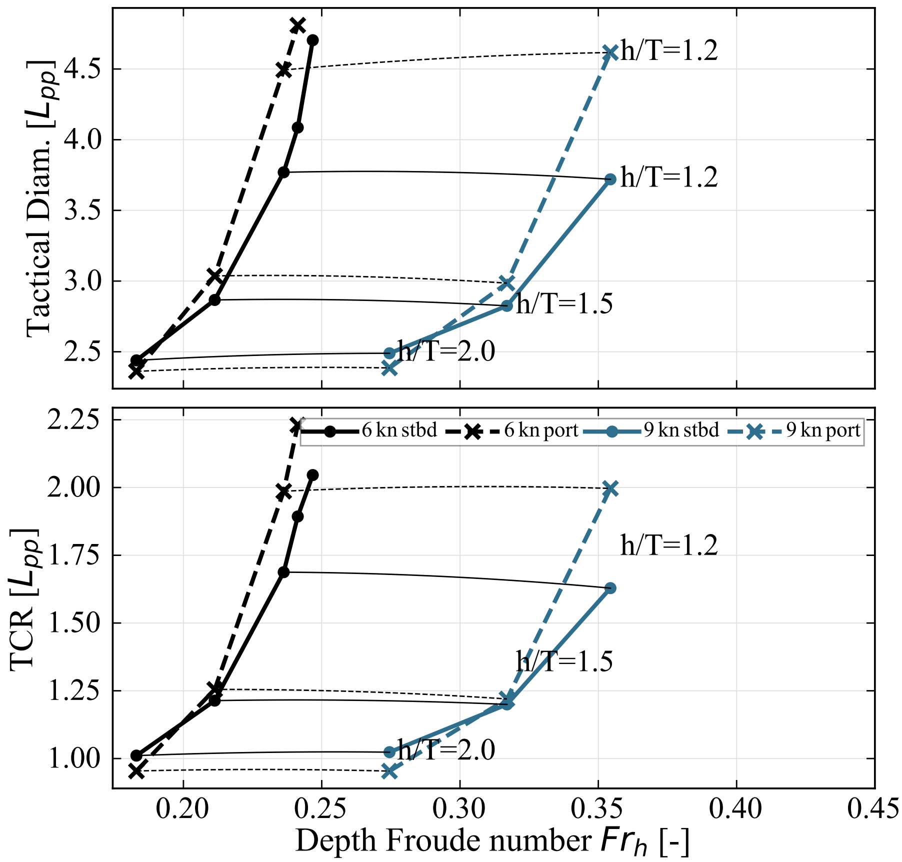

Fig. 13. Tactical diameter and turning circle radius of the 45° turning circle manoeuvre.

A notable feature is the asymmetric turning behaviour between port and starboard directions. While port turning initially results in smaller diameters under deep- and moderate shallow-water conditions, a reversal occurs as h/T decreases. This trend reversal is particularly pronounced between $h/T = 1.50$ and 1.20, where port-side parameters increase more strongly.

This asymmetry is primarily attributed to propeller–rudder interaction. Shallow-water confinement modifies the inflow to the propeller and alters the resulting asymmetric pressure distribution at the stern of the hull. Furthermore, the restricted inflow and changing wake fraction along the vertical direction of the propeller affect both the asymmetric propeller forces and the inflow to the rudder.

At $h/T = 1.20$, comparable transverse rudder forces are observed for both turning directions, while the longitudinal force remains higher for starboard turning. At the same time, a larger drift angle occurs for starboard turning, leading to stronger deceleration. As a result, similar yaw rates produce smaller turning radii for starboard manoeuvres.

These asymmetries increase with depth Froude number and are further influenced by higher propeller thrust during port-side manoeuvres at $h/T \leq 1.50$, contributing to higher steady velocities. The trend reversal is even more pronounced for the 45° turning circle manoeuvres, where it appears already at $h/T = 1.50$ (Fig. 13).

In summary, shallow-water conditions significantly reduce turning ability and introduce pronounced asymmetric and non-linear effects depending on depth Froude number. These are governed by the interaction between increased hydrodynamic damping and modified propeller–rudder inflow, with the latter playing a key role in determining both velocity loss and yaw response.

After analysing primarily the steady-state characteristics of the turning circle, the transient phases of the manoeuvre are examined in more detail, with emphasis on those features that differ fundamentally from the steady behaviour. To provide a physics based interpretation, CFD results are used to analyse the temporal evolution of the forces acting on the ship during the manoeuvre. The transverse force components along the hull – decomposed into hydrodynamic, rudder, centrifugal, and inertia contributions – are evaluated as a function of heading angle for a 35° turning circle, see Fig. 14.

At the onset of the manoeuvre (phase 1), the motion is dominated by inertia effects induced by the rapidly increasing rudder force. At this stage, both sway and yaw velocities are still negligible, and consequently centrifugal and hydrodynamic forces remain small. The lateral acceleration is therefore governed almost entirely by the rudder action. With decreasing under-keel clearance, however, hydrodynamic damping becomes effective already at very small heading angles. This leads to a pronounced reduction in initial acceleration: even at minimal heading deflections, the inertia forces in deep water are significantly larger than those in extreme shallow water. The increased damping in shallow water therefore suppresses the early development of lateral motion.

During the subsequent transient phase (phase 2), the interaction between inertia, hydrodynamic, and centrifugal forces becomes more complex. In shallow and extreme shallow water, the inertia force decreases rapidly and changes sign at relatively small heading angles, indicating an early suppression of lateral acceleration. In contrast, in deeper water this transition occurs at larger heading angles, reflecting a more sustained acceleration phase. The hydrodynamic transverse forces exhibit a non-monotonic dependence on water depth. In moderate shallow water, they reach higher levels than in deep water over a large portion of the manoeuvre, whereas in shallow and extreme shallow water they are significantly reduced during most of phase 2. This reduction is primarily associated with the strongly diminished sway

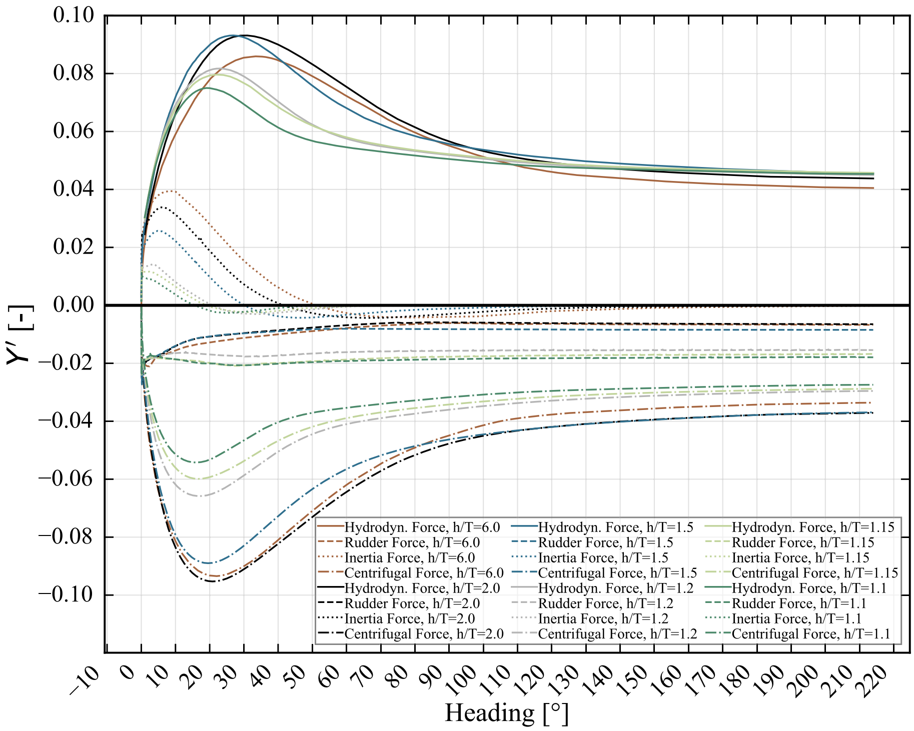

Fig. 14. Force components acting on the DTC during a 35° stbd turning circle manoeuvre with an initial speed of 9 kn at design condition.

velocity resulting from increased damping. At the same time, rudder forces increase substantially with decreasing water depth, particularly under shallow and extreme shallow-water conditions. In contrast, centrifugal forces – which depend on yaw rate – are markedly reduced in shallow water due to the lower rotational velocities. In the most confined condition, their peak values are significantly smaller and are reached earlier compared to deeper water. Overall, the transient dynamics in shallow water are characterized by reduced inertia and centrifugal contributions. During most of phase 2, the hydrodynamic forces are also lower than in deep water, despite the increased damping effects. In moderate shallow water, by contrast, hydrodynamic forces are enhanced and dominate the force balance over a wider range of heading angles.

In the steady phase (phase 3), the behaviour changes fundamentally. Here, hydrodynamic forces increase again with decreasing water depth, exceeding deep-water levels. The lowest steady hydrodynamic forces are observed in deep water, while shallow- and extreme shallow-water conditions exhibit consistently higher values. This reversal compared to the transient phase highlights the fundamentally different force balance governing steady turning motion.

Additional insight into shallow-water effects during the transient phases can be obtained by comparing manoeuvres performed in deep and intermediate water conditions at higher speeds. While transfer and turning radius increase progressively with decreasing h/T, the advance exhibits a non-monotonic behaviour, see Fig. 15. In the transition from deep water to moderate shallow water, a reduction in advance is observed, followed by a subsequent increase at smaller h/T ratios. This behaviour cannot be explained solely by the evolution of drift angle or surge velocity, as both show relatively smooth trends over the same range. Rudder forces are changing only slightly for the transition from deep to moderate shallow water.

Instead, the changes are closely associated with the development of yaw dynamics. In moderate shallow water, higher peak yaw rates are observed during the early stages of the manoeuvre compared to deep water. This leads to an improved initial turning response despite the overall deterioration of steady turning performance at smaller h/T ratios.

Such behaviour suggests that the initial manoeuvring response is governed by changes in the pressure distribution along the hull and the resulting moment development. However, a detailed explanation of these mechanisms requires further analysis of the local flow field, which is addressed in the subsequent sections.

Since the turning motion is governed by the hydrodynamic yaw moment, its spatial distribution along the hull is analysed as a function of heading angle. The CFD results for a 35° starboard turning circle are evaluated by dividing the hull into four longitudinal sections: aft, aft-midship, forward-midship, and fore, see Fig. 16.

The contribution of each section to the total yaw moment varies significantly with both heading angle and water depth. In the following, representative cases for deep water, moderate shallow water (h/T = 2.00), and extreme shallow water (h/T = 1.10) are considered in particular. A negative yaw moment (for starboard turning) opposes the turning motion, whereas a positive contribution promotes it.

In deep and moderate shallow water, the aft section dominates the damping of the turning motion. The corresponding yaw moment increases rapidly with heading angle, reaching a maximum at approximately 35°, and represents the largest opposing contribution. In contrast, under extreme shallow-water conditions, the stern contribution remains comparatively small throughout the manoeuvre. Even in steady turning, the aft-section moment reaches only a fraction of the magnitude observed at the bow, indicating a substantially reduced role in yaw damping.

The behaviour of the fore section shows the opposite trend. In deep water, its contribution initially counteracts the turning motion only at very small heading angles before becoming positive and supporting the turn. With decreasing water depth, however, the range over which the fore section generates opposing yaw moment extends significantly. For h/T = 2.00, this counteracting effect persists up to moderate heading angles, while in extreme shallow water the forebody remains a dominant contributor to yaw damping over a large portion of the manoeuvre.

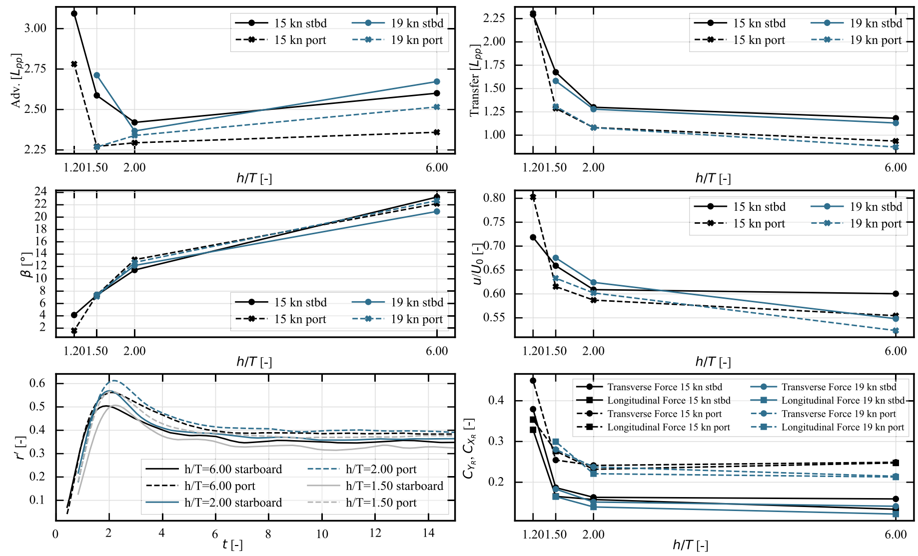

Fig. 15. Turning circle parameters and steady-turning values of drift angle β, speed loss u/U_0, and non-dimensional rudder transverse (C_{Y_R}) and longitudinal (C_{X_R}) force coefficients at 90° heading change, and the time history of the non-dimensional yaw rate r' with an initial speed of 19 kn for the 35° turning circle manoeuvre in deep and shallow water. For comparison, the values for port manoeuvres of β, r' and C_{Y_R} are multiplied by −1.

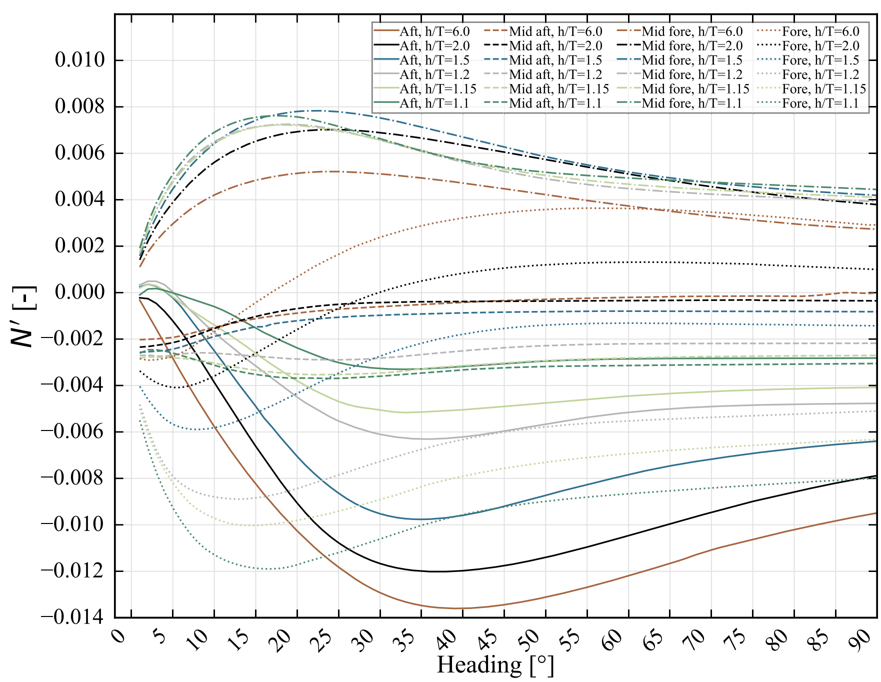

Fig. 16. Calculated hydrodynamic yaw moment as a function of heading angle for different ship sections of the DTC for a 35° stbd turning circle manoeuvre with an initial speed of 9 kn.

The midship sections exhibit more moderate but still relevant contributions. The aft-midship region initially provides damping in all water depths but rapidly decreases towards negligible values in deeper water. In shallow and extreme shallow water, however, it maintains a persistent, albeit moderate, opposing contribution.

The forward-midship section consistently promotes the turning motion across all conditions. Its influence increases strongly in shallow water, particularly at intermediate heading angles, and becomes one of the dominant positive contributors to the yaw moment. In deep water, by comparison, its effect remains relatively weak throughout the manoeuvre.

Overall, a clear redistribution of the yaw moment along the hull is observed with decreasing water depth. The primary source of yaw damping shifts from the stern towards the forebody, while the contribution of the forward-midship region to the turning moment increases. This longitudinal redistribution fundamentally alters the balance of moments governing the manoeuvre and provides a key explanation for the observed changes in turning behaviour under shallow-water conditions.

To further analyse the mechanisms governing the transient behaviour, a representative heading angle of 15° is considered, as this stage is particularly relevant for the initial turning ability. This analysis focuses first on the observed force and moment redistribution before discussing the associated flow mechanisms.

The longitudinal distribution of hydrodynamic transverse forces along the hull reveals a pronounced shift with decreasing water depth,

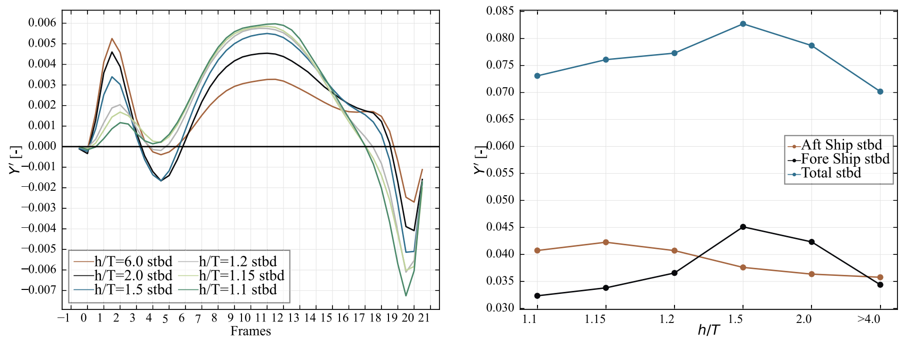

(a) Forces as a function of ship's frames (b) Summed Forces for aft and fore ship

Fig. 17. Hydrodynamic lateral forces for a 35° stbd turning circle manoeuvre with an initial speed of 9 kn at 15° heading change.

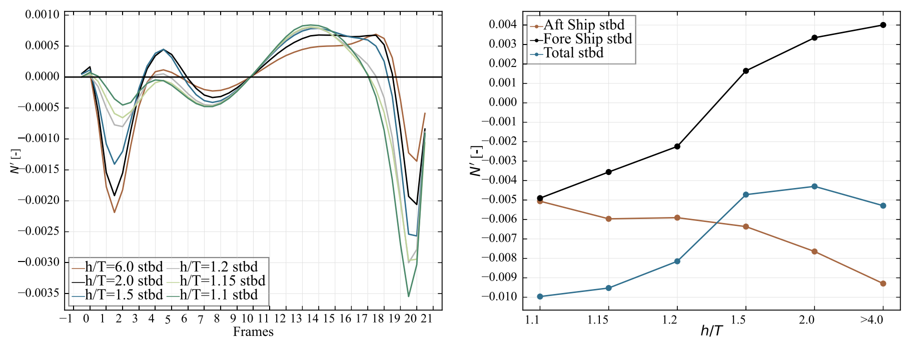

(a) Yaw Moments as a function of ship's frames (b) Summed Yaw Moments for aft and fore ship

Fig. 18. Hydrodynamic yaw moment for a 35° stbd turning circle manoeuvre with an initial speed of 9 kn at 15° heading change.

see Fig. 17(a). In deep water, the force distribution is clearly dominated by the stern, whereas in extreme shallow water it becomes strongly bow-dominated. Notably, the increase in transverse force at the bow exceeds the corresponding reduction at the stern, resulting in a substantially larger transverse force opposing the turning motion under very shallow-water conditions, see Fig. 17(b).

In contrast, the transition from deep to moderate shallow water shows a different behaviour. Here, the transverse forces in the forward midship region – located ahead of the centre of gravity – increase significantly. This leads to an enhanced contribution to the turning moment in this region, partially offsetting the damping contributions from the bow and stern. At the same time, the negative transverse force at the bow and the positive contribution at the stern change in a nearly symmetric manner, maintaining a similar zero-crossing position along the hull. A comparison of the integrated transverse forces confirms that the initial increase in forebody forces in moderate shallow water results in a net increase of assisting hydrodynamic forces.

However, the evaluation of the corresponding yaw moment distribution shows that the overall balance between bow and stern contributions is decisive, see Fig. 18. With decreasing h/T, the yaw moment generated by the forward part of the hull decreases steadily and eventually changes its role. While it supports the turning motion in deep and moderate shallow water, it contributes to damping in shallow and extreme shallow water.

At the same time, the aft section consistently generates a damping moment for all water depths. From deep water to $h/T = 1.20$, this contribution becomes less negative (i.e. weaker damping), before decreasing again towards extreme shallow water. At $h/T = 1.10$, the magnitudes of the forward and aft yaw moments become comparable, indicating a fundamentally altered moment balance along the hull.

Despite the increase in local lateral forces during the transition to moderate shallow water, the total yaw moment of the forebody decreases slightly. However, this reduction is compensated by the increased positive contribution in the forward midship region and the simultaneous weakening of the aft damping moment. As a result, the overall damping moment of the ship is reduced in moderate shallow water, leading to an enhanced initial turning ability compared to deep-water conditions.

A more detailed examination of the longitudinal yaw moment distribution highlights that the regions between frames 3–5.5 and 10–18.5 are primarily responsible for this behaviour. In moderate shallow water, the changes in these regions largely compensate each other, resulting in only minor variations of the total moment. In shallow and extreme shallow water, however, the strong increase of the bow contribution dominates, while the zero-crossing point shifts significantly aft. This shift indicates a substantial redistribution of the force balance along the hull.

The corresponding pressure fields help to explain the previously identified redistribution of yaw moments. The underlying flow mechanisms are reflected in the pressure distribution, see Fig. 19. In extreme shallow water, the stagnation region at the bow shifts laterally, leading to a pronounced increase in positive pressure on the forward shoulder. As a result, the region contributing to a turning-supporting yaw moment is displaced further aft and reduced in magnitude.

In moderate shallow water, the pressure distribution at the bow and stern remains similar to deep-water conditions, whereas the suction region along the midship section intensifies significantly. This behaviour is consistent with the restricted flow beneath the keel and the still pronounced drift angle, which together promote the development of strong negative pressures on the suction side.

With further reduction of water depth, the negative pressure on both the suction and pressure regions increase, and their effects partly compensate each other. Consequently, the net transverse force in the midship region changes only moderately for water depths below moderate shallow-water conditions, despite substantial local pressure variations.

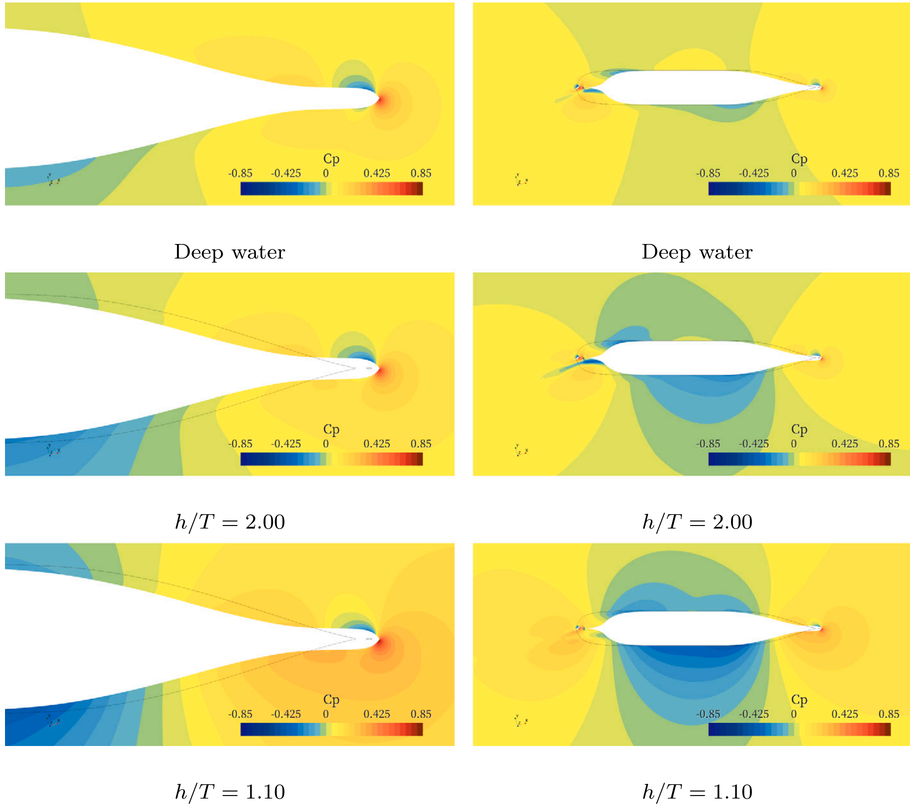

Fig. 19. Pressure distribution at a horizontal plane 9.2 cm below the waterline (corresponding to 5.5 m at full scale) for the bow area (left) and the entire hull (right), shown in terms of the pressure coefficient C_P with the initial straight-ahead speed of 0.6 m/s (corresponding to 9 kn at full scale) as reference speed, for a 15° heading angle at 35° stbd turning circle manoeuvre for the DTC.

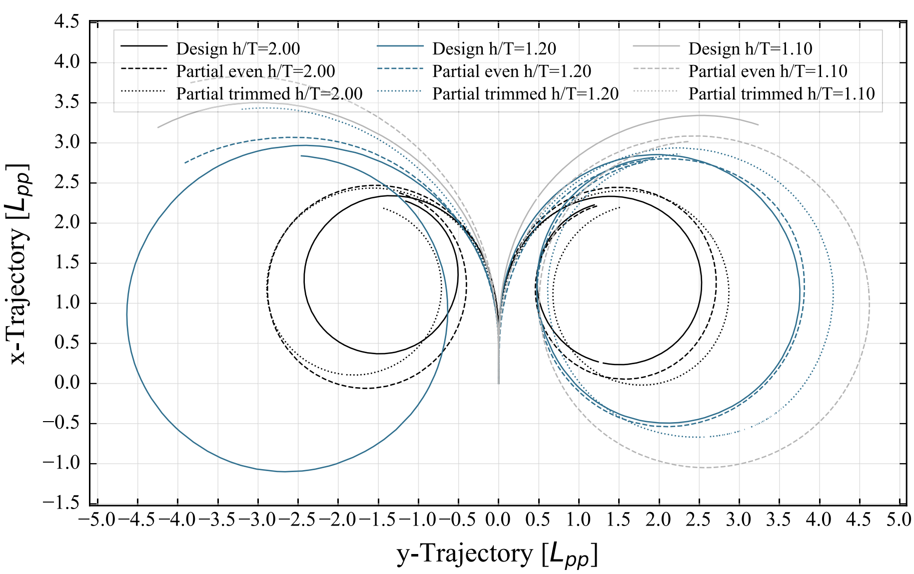

Fig. 20. Trajectories of the 45° turning circle manoeuvre for different floating conditions at 9 kn.

4.2. Floating condition effects on turning behaviour in shallow water

The following section investigates the influence of altered floating conditions on manoeuvring behaviour in shallow water. In addition to the design condition, the ship was examined at a reduced draught of 12.50 m on even keel and with a trim of 2 m by stern. For these off-design conditions, the test matrix was limited compared to the design case, and only h/T ratios of 2.00, 1.20, and 1.10 were considered. It should be noted that the h/T ratio always refers to the mean draught. Consequently, due to the increased draught at the stern, investigations at $h/T = 1.10$ were not feasible for the trimmed condition.

The 45° turning circle manoeuvre was carried out at 6 and 9 kn in starboard direction and at 9 kn in port direction. Therefore, the following analysis focuses on 9 kn. The resulting trajectories for the different floating conditions at h/T ratios of 2.00, 1.20, and 1.10 are presented in Fig. 20. In general, the turning circles in port direction are consistently larger than those to starboard for all off-design conditions and h/T ratios. Already at $h/T = 1.20$, the port trajectories no longer

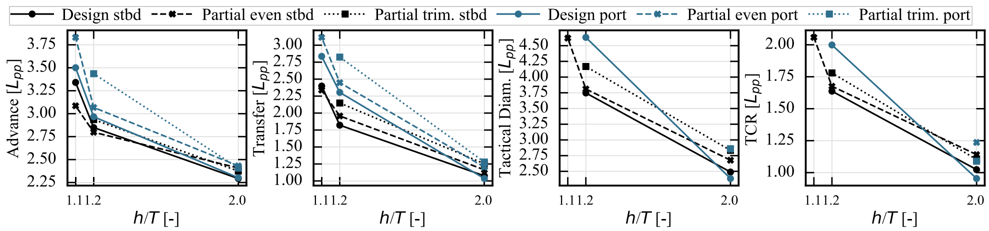

Fig. 21. Turning circle Parameters of 45° turning circle manoeuvre for different floating conditions.

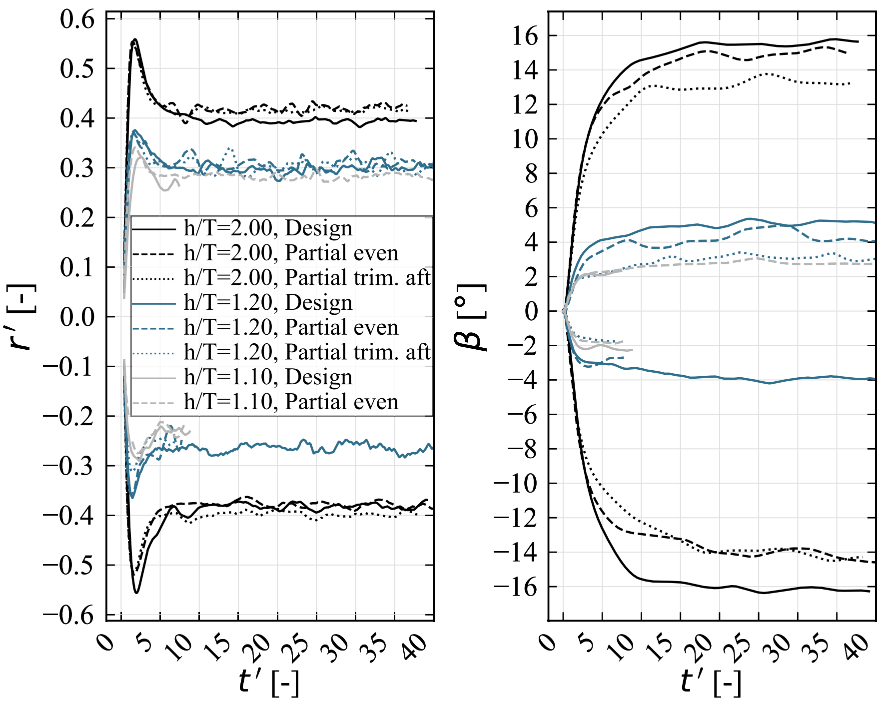

Fig. 22. Yaw rate and drift angle of 45° turning circle manoeuvre for different floating conditions.

fit within the manoeuvring basin, whereas this limitation occurred only at smaller h/T ratios for the design condition. Consequently, the previously observed trend reversal between port and starboard turning with decreasing water depth is no longer present at partial draught, as port-side manoeuvres already exhibit slightly larger characteristic parameters under moderate shallow-water conditions.

For port manoeuvres, only parameters corresponding to a heading change of 90° can be evaluated at lower h/T ratios, see Fig. 21. While the advance at $h/T = 2.00$ is only marginally affected by changes in trim, the influence becomes more pronounced at $h/T = 1.20$. At $h/T = 1.10$, only the effect of reduced draught can be assessed. Here, the directional asymmetry in the advance increases at partial draught, with the magnitude of this increase becoming more significant as h/T decreases.

The turning circle radius at partial draught for starboard direction approaches that of the design condition with decreasing h/T, and becomes even smaller at $h/T = 1.10$, allowing the trajectory to remain within the basin under these extreme shallow-water conditions. In starboard direction, the influence of draught on the turning circle thus differs from that observed in port direction. In contrast, the transfer shows a comparable sensitivity to floating condition in both directions, with the largest increase occurring for the trimmed condition.

The drift angle in starboard direction (Fig. 22) is only slightly reduced for partial draught on even keel compared to the design condition at $h/T = 2.00$ and 1.20. When trimmed by stern, the drift angle decreases further, reaching values approximately 20% lower at $h/T = 2.00$ and up to 50% lower at $h/T = 1.20$ compared to the design condition. For trimmed conditions at $h/T = 1.20$, the drift angle is comparable to that at $h/T = 1.10$ for even keel at partial draught, despite a turning circle radius that is approximately 15% smaller. The sensitivity of drift angle to trim increases with decreasing water depth. Overall, the influence of water depth is more significant than that of draught variation.

The steady yaw rate is comparatively less affected by these variations in drift angle, see Fig. 22. The maximum yaw rate occurs in moderate shallow water for all floating conditions. While the overall trends remain similar, the influence of water depth becomes more pronounced, particularly in the transition from moderate shallow to shallow water. In steady-state conditions, partial draught generally results in similar or slightly higher yaw rates compared to the design condition.

In summary, reduced draught enhances the asymmetry of turning behaviour with decreasing water depth. The improvement in turning ability for starboard manoeuvres and the simultaneous deterioration for port manoeuvres become more pronounced, particularly in terms of advance. Trim by stern further reduces turning performance and significantly affects the drift angle, with its influence increasing as water depth decreases.

5. Conclusion

The present study examined the turning behaviour of a container vessel in shallow water using a combined experimental and CFD-based approach, with particular emphasis on the interaction between water depth, ship speed, and the resulting hydrodynamic force distribution.

Prior to analysing the manoeuvring behaviour, the CFD model was verified through a systematic grid convergence study and validated against model tests for resistance, propulsion, and 35° turning circles at various water depths. The verification demonstrated generally monotonic or oscillatory convergence, confirming the reliability of the numerical setup. Validation showed good agreement with experimental data, with mean deviations of manoeuvring and dynamic parameters close to 5%, confirming that the CFD simulations accurately capture both steady and transient shallow-water effects.

Consistent with established knowledge, a reduction in water depth leads to a deterioration of steady turning performance, reflected in increasing tactical diameters and decreasing yaw rates. As outlined in previous studies, these effects are commonly attributed to increased hydrodynamic damping. The present results confirm this interpretation, but further show that the underlying mechanisms are governed by a depth-dependent redistribution of forces along the hull.

The main findings can be summarized as follows:

- The longitudinal distribution of transverse forces changes fundamentally, shifting from a stern-dominated to a bow-dominated pattern with decreasing h/T. This redistribution governs the development of the hydrodynamic yaw moment and explains both steady-state and transient manoeuvring behaviour.
- A clear water-depth-dependent asymmetry between port and starboard turning manoeuvres is observed, which reverses with decreasing water depth. This behaviour is linked to the interaction between propeller rotation, rudder inflow, and the depth-dependent modification of the wake field, resulting in differences in drift angle, surge velocity, and yaw moment.
- An improved initial turning ability was identified for moderate shallow water conditions. This enhancement at $h/T \approx 2.00$ results from increased forward-midship contributions and reduced stern damping.
- Extreme shallow water ($h/T = 1.10$) exhibits a sharp decline in initial turning ability, contrasting with the moderate increase observed in the transition from $h/T = 1.20$ to 1.15, thereby identifying a critical threshold.
- Depth Froude number strongly influences manoeuvring behaviour, particularly at higher speeds, where non-linear interactions between surge velocity, propeller inflow, and rudder forces lead to pronounced deviations in yaw rate and advance during turning.
- Floating condition (draught and trim) significantly affects shallow-water turning behaviour, increasing directional asymmetry and reducing turning ability for stern-trimmed conditions, primarily through its influence on drift angle, with effects intensifying at lower h/T ratios.

Overall, the study establishes a direct link between depth Froude number, local hydrodynamic force redistribution, and global manoeuvring behaviour. In particular, the identification of a critical threshold at extreme shallow-water conditions and the reversal of directional asymmetry provide new insight into the governing mechanisms of ship turning in confined environments.

However, as the present investigation is limited to a single container-vessel with a specific stern and rudder arrangement, the quantitative extent of these effects may vary for other ship types. Further investigations are therefore required to assess the general applicability of the identified trends. Nevertheless, the presented results provide valuable physical insight into shallow-water manoeuvring behaviour and the associated hydrodynamic mechanisms. They thereby contribute to an improved understanding of ship manoeuvring in confined waterways and support the development of more reliable prediction methods for safe ship operations in restricted waters.

The identified sensitivity of turning behaviour to depth Froude number, water depth, and floating condition demonstrates that manoeuvring performance in shallow water cannot be reliably assessed based on isolated operating conditions. In particular, the observed changes in directional asymmetry, yaw response, and initial turning ability are directly relevant for manoeuvring prediction methods and simulator models used for restricted-water operations. Furthermore, the identified deterioration of turning performance and the strong increase in advance under extreme shallow-water conditions provide important information for the assessment of manoeuvring margins and the dimensioning of navigation channels. The demonstrated redistribution of hydrodynamic forces and yaw moments along the hull additionally provides valuable insight for the development of more physics-based manoeuvring and control models. In combination with the identified transition towards extreme shallow-water conditions, characterized by abrupt changes in manoeuvring response, these findings may also support future autonomous or assisted navigation systems operating under strongly non-linear shallow-water conditions.

CRediT authorship contribution statement

Marcus Döscher: Writing – review & editing, Writing – original draft, Visualization, Validation, Methodology, Investigation, Formal analysis, Data curation, Conceptualization. **Carl-Uwe Böttner:** Writing – review & editing, Supervision, Resources, Project administration, Methodology, Funding acquisition. **Moustafa Abdel-Maksoud:** Writing – review & editing, Supervision, Methodology, Formal analysis, Conceptualization.

Declaration of competing interest

The authors declare that they have no known competing financial interests or personal relationships that could have appeared to influence the work reported in this paper.

Acknowledgments

This work was carried out within the departmental research and development programme of the Federal Waterways Engineering and Research Institute (Bundesanstalt für Wasserbau, BAW), funded by the German Federal Ministry of Transport. The contributions of the experimental team at the BAW model test facilities are gratefully acknowledged.

References

Bogdanov, P., Vassilev, P., Lefterova, M., Milanov, E., 1987. "Esso osaka" tanker manoeuvrability investigations in deep and shallow water, using PMM. Int. Shipbuild. Prog. 34 (390), 30–39. http://dx.doi.org/10.3233/ISP-1987-3439002.

Carrica, P.M., Mofidi, A., Eloot, K., Delefortrie, G., 2016. Direct simulation and experimental study of zigzag maneuver of KCS in shallow water. Ocean Eng. 112, 117–133. http://dx.doi.org/10.1016/j.oceaneng.2015.12.008.

EMSA, 2022. Safety Analysis of EMCIP Data: Analysis of Navigation Accidents. V1.0. URL https://www.emsa.europa.eu/newsroom/latest-news/item/4830-safety-analysis-of-emcip-data-analysis-of-navigation-accidents.html,

He, S., Kellett, P., Yuan, Z., Incecik, A., Turan, O., Boulougouris, E., 2016. Manoeuvring prediction based on CFD generated derivatives. J. Hydrodyn. 28 (2), 284–292. http://dx.doi.org/10.1016/S1001-6058(16)60630-3.

ITTC (Ed.), 2008. Proceedings of the 25th International Towing Tank Conference (Vol. 1): The Manoeuvrability Comittee - Final Report and Recommendations to the 25th ITTC. ITTC.

ITTC (Ed.), 2014. Recommended Procedures and Guidelines: Captive Model Test Procedure.

ITTC (Ed.), 2021. Recommended Procedures and Guidelines: Free Running Model Tests.

ITTC (Ed.), 2024. Recommended Procedures and Guidelines: Uncertainty Analysis in CFD Verification and Validation Methodology and Procedures.

Jansch, H., Böttner, C.-U., 2019. Sea trials for determination of manoeuvring characteristics in shallow water conditions. URL https://hdl.handle.net/20.500.11970/107126.

Jiao, J., Ren, H., Guedes Soares, C., 2021. A review of large-scale model at-sea measurements for ship hydrodynamics and structural loads. Ocean Eng. 227, 108863. http://dx.doi.org/10.1016/j.oceaneng.2021.108863.

Kim, D., Tezdogan, T., Incecik, A., 2022. Hydrodynamic analysis of ship manoeuvrability in shallow water using high-fidelity URANS computations. Appl. Ocean Res. 123, 103176. http://dx.doi.org/10.1016/j.apor.2022.103176.

Lee, S., Hong, C., 2017. Study on the course stability of very large vessels in shallow water using CFD. Ocean Eng. 145, 395–405. http://dx.doi.org/10.1016/j.oceaneng.2017.09.064.

Li, Y., Landsburg, A.C., Barr, R.A., Calisal, S.M., 2006. Improving ship maneuverability standards as a means for increasing ship controllability and safety. In: Oceans 2005. IEEE Operations Center, Piscataway, NJ, pp. 1–10. http://dx.doi.org/10.1109/OCEANS.2005.1640048.

Liu, Y., Zou, Z.J., Zou, L., 2016. RANS-based numerical simulation of captive model tests in shallow water for the DTC container carrier. In: Uliczka, K., Böttner, C.-U., Kastens, M., Eloot, K., Delefortrie, G., Vantorre, M., Candries, M., Lataire, E. (Eds.), 4th MASHCON - International Conference on Ship Manoeuvring in Shallow and Confined Water with Special Focus on Ship Bottom Interaction. Bundesanstalt für Wasserbau, Karlsruhe, http://dx.doi.org/10.18451/978-3-939230-38-0_10.

Liu, Y., Zou, Z., Zou, L., Fan, S., 2019. CFD-based numerical simulation of pure sway tests in shallow water towing tank. Ocean Eng. 189, 106311. http://dx.doi.org/10.1016/j.oceaneng.2019.106311.

Lu, H.S., Chu, W.W., Fei, N.Z., Wang, W.F., 1987. Some results from free-sailing model tests on water depth effect on manoeuvring performance. In: ITTC (Ed.), Proceedings of the 18th International Towing Tank Conference (Vol. 2) - Session on Manoeuvrability. pp. 215–217.

Milanov, E.M., Chotukova, V.Y., 2009. Roll motion of containership in shallow water. In: Eloot, K., Vantorre, M. (Eds.), International Conference on Ship Manoeuvring in Shallow and Confined Water: Bank Effects. The Royal Institution of Naval Architects, London, pp. 99–104. http://dx.doi.org/10.3940/rina.bank.2009.10.

Moctar, O.e., Shigunov, V., Zorn, T., 2012. Duisburg test case: Post-panamax container ship for benchmarking. Ship Technol. Res. 59 (3), 50–64. http://dx.doi.org/10.1179/str.2012.59.3.004.

Neitzel, J.C., Pergande, M., Berger, S., Abdel-Maksoud, M., 2015. Influence of the numerical propulsion modelling on the velocity distribution behind the propulsion device and maneuvering forces. In: Fourth International Symposium on Marine Propulsors Smp'15.

Ohmori, T., 2024. Viscours flow simulation of KVLCC2 in shallow water. In: SIMMAN 2020: Workshop on Verification and Validation of Ship Manoeuvring Simulation Methods: Workshop Proceedings.

PIANC, 1992. Capability of ship manoeuvring simulation models for approach channels and fairways in harbours: Report of working group no. 20 of permanent technical committee II. In: Supplement to Bulletin 77, Permanent International Association of Navigation Congresses, Bruxelles.

RoyChoudhury, S., Dash, A.K., Nagarajan, V., Sha, O.P., 2017. CFD simulations of steady drift and yaw motions in deep and shallow water. Ocean Eng. 142, 161–184. http://dx.doi.org/10.1016/j.oceaneng.2017.06.058.

Schmidt-Stiebitz, H., 1958. Forschungsberichte des Wirtschafts- und Verkehrsministeriums Nordrhein-Westfalen Nr. 476: Einflußder Hinterschiffsform auf das Manövrieren von Schiffen auf flachem Wasser. Westdeutscher Verlag, Köln und Opladen.

Toxopeus, S.L., 2013. Viscous-flow calculations for KVLCC2 in deep and shallow water. In: Eça, L., nate, O., Eugenio, García-Espinosa, J., Kvamsdal, T., Bergan, P. (Eds.), MARINE 2011, IV International Conference on Computational Methods in Marine Engineering. In: Computational Methods in Applied Sciences, vol. 29, Springer, Dordrecht, pp. 151–169. http://dx.doi.org/10.1007/978-94-007-6143-8_9.

Wang, H.M., Chen, X.Y., Yu, H.M., Chen, L., Wang, T., Xu, J.R., Wang, X.F., 2023. Numerical simulation of the viscous flow around ships turning in shallow water. Int. J. Marit. Eng. 164 (A3), http://dx.doi.org/10.5750/ijme.v164iA3.1242.

Xing, T., Stern, F., 2010. Factors of safety for richardson extrapolation. J. Fluids Eng. 132 (6), http://dx.doi.org/10.1115/1.4001771.

Yun, K., Yeo, D.J., Park, B., 2015. A study on the manoeuvrability of KVLCC2 in shallow water by free running model test. J. Soc. Nav. Archit. Korea 52 (6), 494–500. http://dx.doi.org/10.3744/SNAK.2015.52.6.494.